



Boron Doped ZnO Films Deposited by DC Reactive Sputtering Using Zn:B Target: Influence of the Deposition Temperature on the Structural, Electrical and Optical Properties

Lwitiko P. Mwakyusa*, Nuru R. Mlyuka and Margaret E. Samiji

Department of Physics, University of Dar es Salaam, P.O. Box 35063, Dar es Salaam, Tanzania

Corresponding author, e-mail: mwakyusa.lwitiko@udsm.ac.tz

Received 18 Nov 2021, Revised 24 Mar 2022, Accepted 26 Mar 2022, Published Mar 2022

DOI: <https://dx.doi.org/10.4314/tjs.v48i1.14>

Abstract

ZnO-based transparent and conducting oxides (TCOs) are commonly used as a window layer in thin-film solar cells. However, TCOs with high transparency in the visible and near-infrared parts of the electromagnetic spectrum, plus excellent electrical properties are required in this application. In this study, TCOs based on ZnO:B films deposited by DC reactive sputtering using Zn:B alloy target were investigated. The impact of deposition temperature on the growth and physical properties of the films was examined. Structural, optical and electrical properties of these films were investigated by means of x-ray diffraction (XRD), Ultraviolet-Visible-Near Infrared (UV-VIS-NIR) spectroscopy, and Hall effect measurement, respectively. The XRD analysis revealed that all films are of hexagonal wurtzite structures, with a preferred orientation along the *c*-axis. The optical spectroscopy results indicated that all the ZnO:B films had optical transparency above 90% in the visible region which then slightly decreased in the near-infrared region. The highest carrier concentration, conductivity, and mobility were obtained at the deposition temperature of 300 °C—due to improvement in crystal growth—while higher temperatures slightly deteriorated the electrical properties, possibly due to a slight decrease in the crystallite size.

Keywords: ZnO; Transparent and conducting oxides; ZnO:B, DC reactive sputtering; deposition temperature.

Introduction

Zinc oxide (ZnO) is a very promising group II-VI compound semiconductor as a window layer for thin-film solar cell applications since it is comprised of earth-abundant and non-toxic elements. Furthermore, it has a wide direct optical bandgap (~3.37 eV) with a large exciton binding energy of 60 meV at room temperature (Pawar et al. 2009, Pholds et al. 2016). The optical, electrical and structural properties of ZnO films are attributed to the presence of intrinsic native defects such as oxygen vacancies and zinc ions interstitials (Pawar et al. 2005, Tahar and Tahar 2005,

Kim et al. 2009b). However, at room temperature, these defects are not stable (Kim et al. 2009a). As a result, ZnO becomes unstable and its conductivity decreases by several orders of magnitude at room temperature (Kim et al. 2009a, Maloda and Malisa 2020). Experimentally, it has been proved that partial substitution of Zn with group IIIA elements (B, Al, Ga, and In) improves both stability and optoelectronic properties of ZnO films (Tahar and Tahar 2005, Kim et al. 2009a, Pholds et al. 2016). Considerable attention has been dedicated to partial substitution of Zn with Al. By using this approach, a transparent conducting oxide

with resistivity below 10^{-4} $\Omega\cdot\text{cm}$ with average visible transmittance of 88% was demonstrated (Agura et al. 2003). Aluminium doped ZnO is currently used as a transparent window layer in thin-film-based photovoltaic (PV) technologies (Hagiwara et al. 2001, Mwakyusa et al. 2019, Mwakyusa et al. 2020). For instance, CIGS solar cells with efficiencies of up to 23.2% are demonstrated when Al-doped ZnO (ZnO:Al) film is utilized as window layer (Green et al. 2021). However, ZnO:Al films exhibit an absorption loss in the near-infrared region, which results to a decrease in the short-circuit current (J_{sc}) of a solar cell (Pholds et al. 2016, Hagiwara et al. 2001). Hagiwara et al. (2001) experimentally revealed an improvement of J_{sc} CIGS devices when DC sputtered ZnO:B film was utilized as a window layer. The window layer deposition was carried out in the B_2H_6 -Ar mixture. Meanwhile, Kim et al. (2009a) suggested that it is possible to prepare high transparency textured ZnO:B films by low-pressure chemical vapor deposition (LPCVD). A similar approach was also reported by Li et al. (2020). In both cases, toxic diborane (B_2H_6) gas was utilized as a source of B dopant. On the other hand, ZnO:B films with resistivity of 7.5×10^{-3} $\Omega\cdot\text{cm}$ deposited by RF sputtering of high-purity ZnO: B_2O_3 (4 wt%) target was reported by Gao et al. (2011). We have previously demonstrated the influence of B doping level on the properties of DC sputtered ZnO:B films using Zn:B (0.5 wt%) alloy target. With the use of this approach, ZnO:B films with resistivity in order of 10^{-3} $\Omega\cdot\text{cm}$ could be demonstrated (Pholds et al. 2016). However, it is well known that the properties of TCO films depend on the deposition conditions (Nsimama and Samiji 2010). It has been shown that deposition temperature is one of the most critical parameters in controlling the crystallization of ZnO:B films (Hagiwara et al. 2001, Chang and Hon 2001, Chen et al. 2005, Rozati and Akeste 2008, Kim et al. 2009a, Mosbah and Aida 2012). It is good to note that these films were prepared using different deposition techniques. However, a similar effect on the DC sputtered ZnO:B films is expected.

However, the impact of deposition temperature on the properties of DC reactive sputtered ZnO:B films using alloy target is not yet investigated. In the present work, we shed some light on the influence of deposition temperature on the properties of DC sputtered ZnO:B films. A clear connection between the structural, optical and electrical properties is elucidated.

Materials and Methods

ZnO:B films fabrication

ZnO:B films were deposited onto soda-lime glass (SLG) substrates via a DC reactive magnetron sputtering in a BALZERS BAE 250 coating unit utilizing an alloy Zn:B (0.5 wt%, size: 5.08 cm diameter \times 0.635 thickness) target with a purity of 99.99% supplied by Plasmaterials Inc. After ultrasonically cleaning the substrate, the SLG substrates were loaded into the sputtering chamber. The distance between the target and the substrate was set to 16 cm. Prior to deposition, the sputtering unit was evacuated to a base pressure of around 10^{-5} mbar. During deposition, Ar and O_2 gas flow rates were fixed at 75 sccm and 4.07 sccm, respectively. The working pressure was fixed at 6×10^{-3} mbar and DC sputtering power was maintained at 120 W. All the samples were deposited for 30 min with the goal of achieving 400 nm film thickness. A detailed description of this approach is found in our previous work (Pholds et al. 2016, Samwel et al. 2015). To investigate the effect of deposition temperature and the properties of ZnO:B films, the substrates were subjected to temperatures of 150 $^\circ\text{C}$, 200 $^\circ\text{C}$, 270 $^\circ\text{C}$, 300 $^\circ\text{C}$, and 370 $^\circ\text{C}$. After deposition, the developed films were allowed to naturally cool down to room temperature under vacuum.

Characterization

The film thickness was determined by post-deposition measurements using the Alpha step IQ profilometer. Phase identification was carried out using Bruker AXS D8 diffractometer system with a Cu $\text{K}\alpha_1$ ($\lambda = 1.540629$ \AA) radiation operated at 40 mA and 40 kV with Bragg-Brentano θ - 2θ

scanning mode. The crystalline phases were analyzed by comparing the measured Bragg diffraction peaks with the cards provided by ICDD. The crystallite size was estimated as ascribed in Pholds et al. (2016). Using origin Pro 2018 software, the value of Full Width at Half Maximum (FWMH) of the dominant XRD peak was evaluated. The electrical properties were analyzed using the Ecopia HMS 3000 Hall measurement system with a 0.56 T magnetic flux. Optical transmittance was measured by using a UV-VIS-NIR double beam spectrophotometer (Varian Carry 5000) in the wavelength range $300 \text{ nm} \leq \lambda \leq 2000 \text{ nm}$ at room temperature. Scout software (2.4, WTheiss Hardware and Software) was used to estimate optical constants of DC sputtered ZnO:B films as ascribed by Cunha et al. (2020).

Results and Discussion

To understand the main material phases of DC sputtered ZnO:B films, XRD measurements were performed and analyzed. The XRD patterns for ZnO:B films prepared with different deposition temperatures are shown in Figure 1(a). As it can be seen, the films are composed mainly of (002) XRD peaks (ICCD No: 36-14-51). No phases related to B_2O_3 or metallic Zn were observed. These suggest that ZnO:B films developed are single-phase hexagonal wurtzite structures and are orientated with the c -axis perpendicular to the substrate. We noticed that the XRD peak (002) intensity improved with the increase in deposition temperature. Using the Gaussian fit, the Full Width at Half Maximum (FWHM) values of (002) peak were extracted (see Figure 1(b)). The FWHM value decreased with increase in the deposition temperature from $150 \text{ }^\circ\text{C}$ to $300 \text{ }^\circ\text{C}$. This indicates the enhancement of the

crystallinity of ZnO:B films when deposition temperature increases. Further increase in the deposition temperature beyond $300 \text{ }^\circ\text{C}$, however, leads to an increase in the FWHM. The average crystallite size of the ZnO:B films were computed from the FWHM of the dominant peak using Scherrer equation as ascribed by Mosbah and Aida (2012) and Maloda and Malisa (2020).

$$D = \frac{k\lambda}{\Delta(2\theta) \cos \theta} \quad (1)$$

where D , λ , θ , and $\Delta(2\theta)$ are respectively, crystallite size, X-ray wavelength, the Bragg diffraction angle and the FWHM in radians. A constant k , depends on the crystallite's shapes (0.9 values were employed in our work assuming spherical crystallites). The dependence of the crystallite size on the deposition temperature is shown in Figure 1 (b) (red line). The crystallite size increases from 8.2 nm to 19.4 nm as the substrate temperature increased from $150 \text{ }^\circ\text{C}$ to $300 \text{ }^\circ\text{C}$. Further increase in substrate temperature beyond $300 \text{ }^\circ\text{C}$ results to a decrease in the crystallite size. These results are in good agreement with those reported for DC sputtered AZO films (Agura et al. 2003, Kim et al. 2009b). Looking at the position of (002) peak relative to that of the ZnO powder (ICCD No: 36-14-51), the peak is shifted toward larger 2θ Bragg's angle. This could be attributed to i) the increase in the lattice parameters due to the incorporation of B^{3+} ions in the interstitial position (Agura et al. 2003, Pholds et al. 2016), ii) the increase in the oxygen vacancies (Agura et al. 2003), and iii) the strain effect due to the thermal expansion coefficient mismatch between the ZnO:B film and the SLG substrate (Agura et al. 2003, Mosbah and Aida 2012).

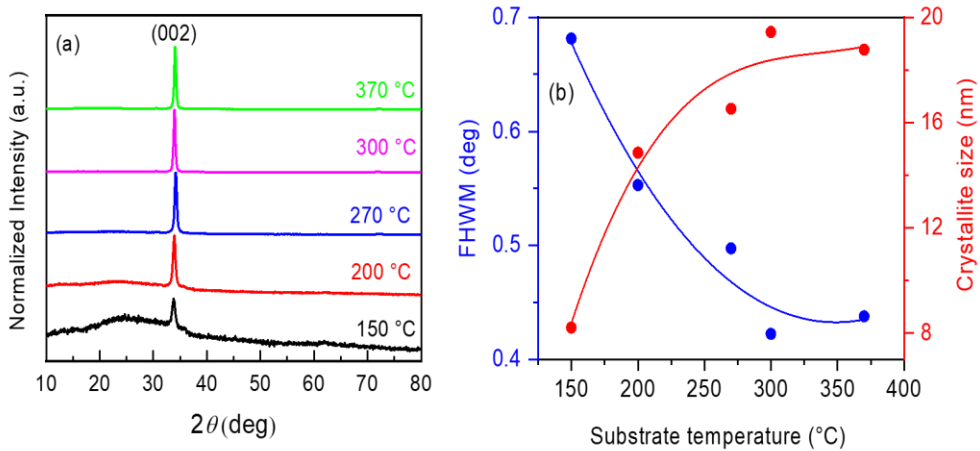


Figure 1: (a) XRD pattern (b) the FWHM of the (002) peak and crystallite size of the ZnO:B films prepared at 150 °C, 200 °C, 270 °C, 300 °C, and 370 °C substrate temperatures.

Having investigated the influence of deposition temperature on the structural properties of the sputtered ZnO:B films, we now describe its impact on the optical properties of the films. Figure 2 (a) depicts the dependence of the optical transparency of a ZnO:B film on the deposition temperature in the wavelength range $320 \text{ nm} \leq \lambda \leq 2000 \text{ nm}$. All ZnO:B films have high optical transparency above 90% in the visible range with a sharp absorption edge in the UV region. It should be noted that high

transparency is an important factor for the material to be used as a window layer in thin-film solar cells. It is well known that the deposition temperature influences the optical constants, n and k of TCOs films. Using Scout simulation software, n and k values were determined, as illustrated in Figure 3. Captivatingly, the optical constants stayed almost constant for all samples. This suggests that the deposition temperature does not significantly impact the dielectric properties of ZnO:B films.

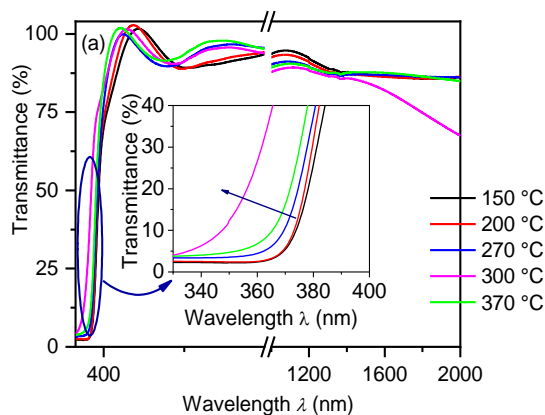


Figure 2: Transmittance spectra of ZnO:B films deposited at different substrate temperatures. The insert shows the absorption edge shift with change in deposition temperature.

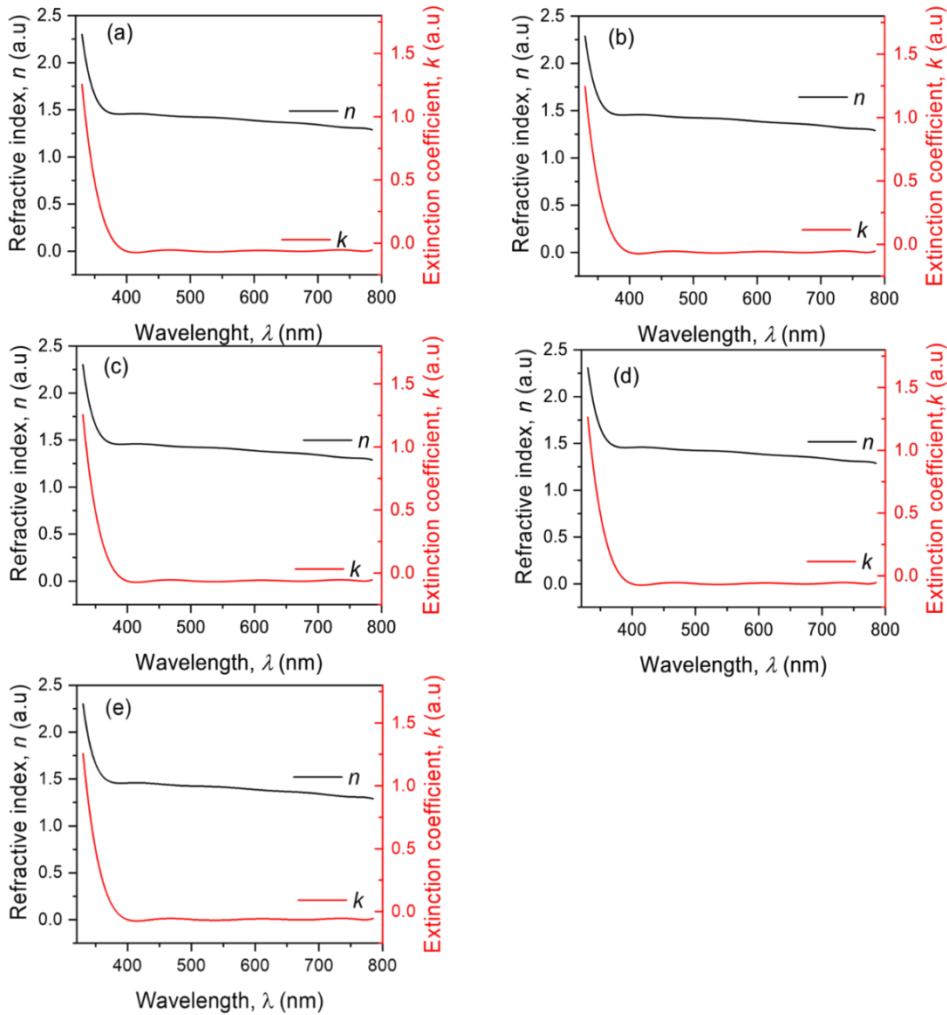


Figure 3: Refractive index n (black line) and extinction coefficient k (red line) as a function of wavelength for ZnO:B films prepared at different temperature: (a) 150 °C, (b) 200 °C, (c) 270 °C, (d) 300 °C, and (e) 370 °C.

Regarding the absorption shift, as can be seen in Figure 2(b), the absorption edge shifted to a shorter wavelengths as the deposition temperature increased from 150 °C to 300 °C before shifting back to a higher wavelength for deposition temperatures above 300 °C. It is often assumed that such a shift is associated with an increase or decrease in the optical bandgap of doped TCOs. The former is due to the Burstein-Moss (B-M) shift effect (Alnajjar 2012). To further address this aspect, the optical bandgap of DC sputtered ZnO:B films was extracted using the Tauc plots (see Figure 3

(a)). It was found that the optical band gap increased from 3.24 eV to 3.40 eV for samples prepared at deposition temperatures of 150 °C and 300 °C, respectively, while temperatures above 300 °C tend to decrease the bandgap of the films (see Figure 3(a)). It was theoretically and experimentally proved that, in TCO films with carrier concentrations above the order of 10^{18} cm^{-3} , the Fermi level tends to lie in the conduction band. Consequently, the absorption edge shifts to shorter wavelengths, thus, widening the optical bandgap of TCO films (Maloda and Malisa 2020). We hypothesized that the

observed shift in our samples is due to the Burstein–Moss (B-M) shift effect. As proof of the concept, we investigated the impact of deposition temperature on the electrical properties of DC sputtered ZnO:B films. To end this, Hall effect measurements were performed at room temperature. We first had a look at the relationship between optical bandgap and free carrier concentration. As depicted in Figure 4 (b), extracted optical bandgap varies linearly with free carrier concentration. This suggests that as temperature increase up to 300 °C, more boron atoms substitute Zn atoms in the

mother lattice and generate more free carriers. As a result, the Fermi level shifts inside the conduction band—hence, bandgap widening of ZnO:B films. However, deposition temperature beyond 300 °C fails to activate enough boron atoms—thus, these unactivated atoms generate no free carriers and could act as scattering centers. Based on the findings, we concluded that the blue shift is due to the B-M shift effect. It is good to note that this shift may also be related to strain, stress, and other types of imperfections in the TCO films (Alnajjar 2012).

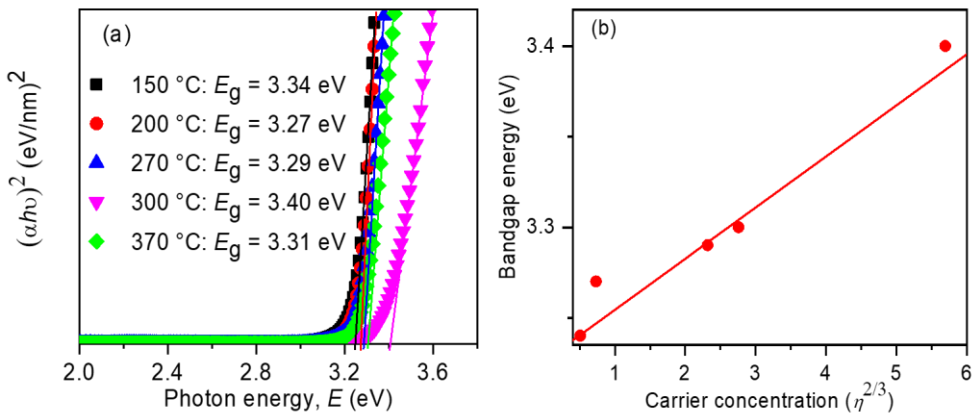


Figure 4: (a) Bandgap estimated by $(\alpha h\nu)^2$ vs E and (b) variation of the optical bandgap with the free carrier concentration of ZnO:B films prepared at 150 °C, 200 °C, 270 °C, 300 °C, and 370 °C substrate temperatures.

Figure 5 shows the dependence of the carrier concentration, mobility, and resistivity of ZnO:B films on the deposition temperature. As illustrated in the Figure 5, the carrier concentration (black line) increased from $1.14 \times 10^{19} \text{ cm}^{-3}$ to $3.7 \times 10^{20} \text{ cm}^{-3}$ as the deposition temperature increased from 150 °C to 300 °C, respectively. Similar observations have been reported in Al-doped ZnO films (Mosbah and Aida 2012, Chang and Hon 2001). This can be explained by the fact that the increase in the deposition temperature enhances activation of B atoms into B^{3+} which is then incorporated in the ZnO lattice, and consequently more extra carriers are generated (Pholds et al. 2016).

Considering the resistivity, ZnO:B films deposited at a temperature around 150 °C

demonstrate the resistivity of $1.9 \times 10^{-1} \Omega\text{-cm}$, increasing the deposition temperature to 300 °C leads to the lowest value of $2.1 \times 10^{-3} \Omega\text{-cm}$, about two orders change. A similar trend can be seen in carrier mobility. This observation is in good agreement with the XRD data. The increase in deposition temperature leads to improvement of the film crystallinity and crystallite size (see Figure 1(b)). Notably, larger crystallite size leads to larger grain size, consequently causing reduction of scattering of the carrier at the grain boundaries and crystal defects (Chen et al. 2005, Kim et al. 2009a, Mosbah and Aida 2012). However, the temperature beyond 300 °C leads to a deterioration of grain size and hence the electrical resistivity and carrier mobility.

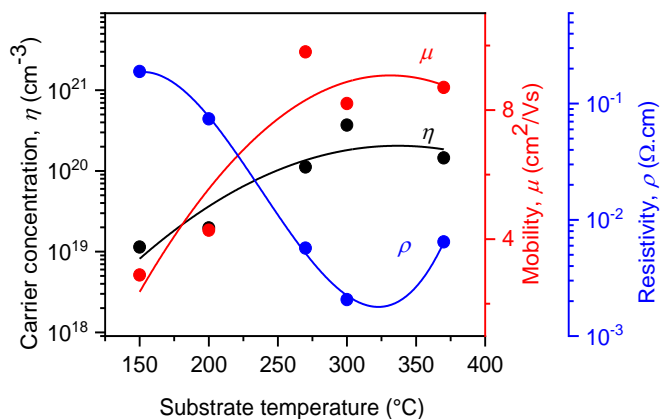


Figure 5: The dependence of the electrical properties of DC sputtered ZnO:B films on the deposition temperature.

Conclusion

In this study, we investigated the influence of deposition temperature on the growth, optical, and electrical properties of DC sputtered ZnO:B-based TCO films. The x-ray diffraction analysis revealed that these films were polycrystalline with (002) a preferable orientation perpendicular to the glass substrate. We further observed that the calculated crystallite size increased from 8.2 to 19.5 nm as temperature increased from 150 °C to 300 °C—while higher temperatures decreased the size. The optimal values of electrical and optical properties were obtained at the deposition temperature of 300 °C. This temperature is a bit higher for ZnO:B films to be utilized as a window layer in thin-film solar cells. Therefore, further optimization is expected to potentially lower the processing temperature and improve other physical properties.

Acknowledgments

LPM gratefully acknowledges SIDA/SAREC through the University of Dar es Salaam (UDSM) for scholarship, and the Royal Society-Leverhulme Trust Africa Award for facilitating a three-month stay for laboratory work at the University of Manchester–UK. The authors thank the International Science Program (ISP) of Uppsala University–Sweden, and the Materials Science and Solar Energy Network for Eastern and Southern

Africa (MSSEESA) for research materials and facilities.

References

- Agura H, Suzuki A, Matsushita T, Aoki T, and Okuda M 2003 Low resistivity transparent conducting Al-doped ZnO films prepared by pulsed laser deposition. *Thin Solid Films* 445(2): 263-267.
- Alnajjar AA 2012 ZnO:Al grown by sputtering from two different target sources: A comparison study. *Adv. Condens. Matter Phys.* 2012: 1-8.
- Chang JF and Hon MH 2001 Effect of deposition temperature on the properties of Al-doped zinc oxide thin films. *Thin Solid Films* 386: 79-86
- Chen X, Guan W, Fang G and Zhao XZ 2005 Influence of substrate temperature and post-treatment on the properties of ZnO:Al thin films prepared by pulsed laser deposition. *Appl. Surf. Sci.* 252(5): 1561-1567.
- Cunha NF, AL-Rjoub A, Rebouta L, Vieira LG and Lanceros-Mendez S 2020 Multilayer passive radiative selective cooling coating based on Al/SiO₂/SiNx/SiO₂/TiO₂/SiO₂ prepared by dc magnetron sputtering. *Thin Solid Films* 694: 137736 (7 pp).
- Gao L, Zhang Y, Zhang J and Xu K 2011 Boron doped ZnO thin films fabricated by RF magnetron sputtering. *Appl. Surf. Sci.* 257(7): 2498-2502.

- Green M, Dunlop E, Hohl-Ebinger J, Yoshita M, Kopidakis N and Hao X 2021 Solar cell efficiency tables (version 57). *Prog. Photovolt.: Res. Appl.* 29(1): 3-15.
- Hagiwara Y, Nakada T and Kunioka A 2001 Improved J_{sc} in CIGS thin film solar cells using a transparent conducting ZnO:B window layer. *Sol. Energy Mater. Sol. Cells* 67(1-4): 267-271.
- Kim G, Bang J, Kim Y, Rout SK and Woo SI 2009a Structural, electrical and optical properties of boron doped ZnO thin films using LSMCD method at room temperature. *Appl. Phys. A* 97: 821-828.
- Kim YH, Lee KS, Lee TS, Cheong B, Seong TY and Kim WM 2009b Effects of substrate temperature and Zn addition on the properties of Al-doped ZnO films prepared by magnetron sputtering. *Appl. Surf. Sci.* 255(16): 7251-7256.
- Li W, Du J, Tang L, Tian Y, Xue F, Jiang Q and Pan S 2020 Influence of boron doping amount on properties of ZnO:B films grown by LPCVD technique and its correlation to a-Si:H/ μ c-Si:H tandem solar cells. *J. Mater. Sci. Mater. Electron.* 31: 6654-6663.
- Maloda E and Malisa A 2020 Influence of deposition temperature on properties of multilayered gallium doped zinc oxide films prepared by dc magnetron sputtering technique. *Tanz. J. Sci.* 46(2): 290-302.
- Mosbah A and Aida MS 2012 Influence of deposition temperature on structural, optical and electrical properties of sputtered Al doped ZnO thin films. *J. Alloys Compd.* 515: 149-153.
- Mwakyusa LP, Leist L, Rinke M, Welle A, Paetzold UW, Richards BS and Hetterich M 2020 Impact of silver incorporation at the back contact of Kesterite solar cells on structural and device properties. *Thin Solid Films* 709: 138223 (10 pp).
- Mwakyusa LP, Neuwirth M, Kogler W, Schnabel T, Ahlswede E, Paetzold UW, Richards BS and Hetterich M 2019 CZTSe solar cells prepared by co-evaporation of multilayer Cu-Sn/Cu,Zn,Sn,Se/ZnSe/Cu,Zn,Sn,Se stacks *Phys. Scr.* 94: 105007 (6 pp).
- Nsimama PD and Samiji ME 2010 Electrical properties of dc reactive magnetron sputtered ZnO: Al films from optical spectra. *Tanz. J. Sci.* 38(2): 39-52.
- Pawar BN, Cai G, D Ham, Mane RS, Ganesh T, Ghule A, Sharma R, Jadhava KD and Han S 2009 Preparation of transparent and conducting boron-doped ZnO electrode for its application in dye-sensitized solar cells. *Sol. Energy Mater. Sol. Cells* 93(4): 524-527.
- Pawar BN, Jadhkar SR and Takwale MG 2005 Deposition and characterization of transparent and conductive sprayed ZnO:B thin film. *J. Phys. Chem. Solids* 66(10): 1779-1782.
- Pholds L, Samiji ME, Mlyuka NR, Richards BS and Kivaisi RT 2016 Boron doped zinc oxide films grown by dc reactive magnetron sputtering. *28th European Photovoltaic Solar Energy Conference and Exhibition (28th EU PVSEC)*: 2311-2315.
- Rozati SM and Akeste Sh 2008 Influence of substrate temperature on the structure of ZnO:Al thin films. *Cryst. Res. Technol.* 43(3): 273-275.
- Samwel B, Samiji ME and Mlyuka NR 2015 Effect of target composition on the optical constants of DC sputtered ZnO:Al thin film. *Tanz. J. Sci.* 41(1): 11-30.
- Tahar RBH and Tahar NBH 2005 Boron-doped zinc oxide thin films prepared by sol-gel technique. *J. Mater. Sci.* 40: 5285-5289.